Journal of Biological Chemistry (2010) 285(32): 24538-24547.

Stable Structural Analog of Ca^<2+>-ATPase ADP-insensitive Phosphoenzyme with Occluded Ca^<2+> Formed by Elongation of A-domain/M1′ -linker and Beryllium Fluoride Binding

Daiho, Takashi ; Danko, Stefania ; Yamasaki, Kazuo ; Suzuki, Hiroshi

Stable Structural Analog of Ca^{2+}-ATPase ADP-insensitive Phosphoenzyme with Occluded Ca^{2+} Formed by Elongation of A-domain/M1'-linker and Beryllium Fluoride Binding*

Takashi Daiho[1], Stefania Danko, Kazuo Yamasaki, and Hiroshi Suzuki

From the Department of Biochemistry, Asahikawa Medical College, Asahikawa 078-8510, Japan

Running Title: *Stable Analog of Transient E2P with Occluded Ca^{2+} in SERCA*

Correspondence address to: Dr. Takashi Daiho, Dept. of Biochemistry, Asahikawa Medical College, Midorigaoka-higashi, Asahikawa, 078-8510, Japan. Tel.: +81 166 68 2353; Fax: +81 166 68 2359
E-mail: daiho@asahikawa-med.ac.jp.

We have developed a stable analog for the ADP-insensitive phosphoenzyme intermediate with two occluded Ca^{2+} at the transport sites ($E2PCa_2$) of sarcoplasmic reticulum Ca^{2+}-ATPase. This is normally a transient intermediate state during phosphoenzyme isomerization from the ADP-sensitive to ADP-insensitive form and Ca^{2+}-deocclusion/release to the lumen; $E1PCa_2 \rightarrow E2PCa_2 \rightarrow E2P + 2Ca^{2+}$. Stabilization was achieved by elongation of the Glu^{40}-Ser^{48} loop linking the Actuator domain and M1 (1st transmembrane helix) with four glycine insertions at Gly^{46}/Lys^{47} and by binding of beryllium fluoride (BeF_x) to the phosphorylation site of the Ca^{2+}-bound ATPase ($E1Ca_2$). The complex $E2Ca_2 \cdot BeF_3^-$ was also produced by lumenal Ca^{2+} binding to $E2 \cdot BeF_3^-$ ($E2P$ ground state analog) of the elongated linker mutant. The complex was stable for at least one week at 25 °C. Only BeF_x, but not AlF_x or MgF_x, produced the $E2PCa_2$ structural analog. Complex formation required binding of Mg^{2+}, Mn^{2+}, or Ca^{2+} at the catalytic Mg^{2+} site. Results reveal that the phosphorylation product $E1PCa_2$ and the $E2P$ ground state (but not the transition states) become competent to produce the $E2PCa_2$ transient state during forward and reverse phosphoenzyme isomerization. Thus isomerization and lumenal Ca^{2+} release processes are strictly coupled with the formation of the acylphosphate covalent bond at the catalytic site. Results also demonstrate the critical structural roles of the Glu^{40}-Ser^{48} linker and of Mg^{2+} at the catalytic site in these processes.

Sarcoplasmic reticulum Ca^{2+}-ATPase (SERCA1a)[2] catalyzes Ca^{2+} transport coupled with ATP hydrolysis (Fig. 1) (1-9). In the catalytic cycle, the enzyme is activated by two cytoplasmic Ca^{2+} ions binding to the transport sites. It is then autophosphorylated at Asp^{351} by MgATP to produce the ADP-sensitive phosphoenzyme ($E1P$) that can react with ADP to regenerate ATP (steps 1-3). $E1P$ formation results in Ca^{2+} occlusion at the transport sites ($E1PCa_2$). Subsequent isomeric transition to an ADP-insensitive form ($E2P$), *i.e.* loss of ADP-sensitivity, results in Ca^{2+} deocclusion and release into the lumen (steps 4-5). This Ca^{2+}-release process is very rapid, so that an $E2PCa_2$ intermediate state does not accumulate and in fact had never been found until we recently established its existence (10-13) and successfully trapped it for the first time (14). The Ca^{2+}-free $E2P$ is finally hydrolyzed to the inactive $E2$ state (steps 6-7). Mg^{2+} as the physiological catalytic cofactor is required for both phosphorylation and hydrolysis. The transport cycle is reversible. Thus $E2P$ can be formed from P_i in the presence of Mg^{2+} and absence of Ca^{2+}. Subsequent Ca^{2+} binding to lumenally oriented low affinity transport sites reverses the Ca^{2+}-releasing step and the $E1P$ to $E2P$ isomerization.

During EP isomerization/Ca^{2+}-release ($E1PCa_2 \rightarrow E2P + 2Ca^{2+}$), the A domain swings around parallel to the membrane plane (*i.e.* horizontal), while the A and P domains and M2 incline and tightly associate (Fig. 2) (15-25). We found that shortening of the A/M1'-linker by deletion of any single residue blocks $E1PCa_2 \rightarrow E2PCa_2$ isomerization and $E2P$ hydrolysis (26). On the other hand, its elongation by two or more glycine insertions markedly accelerates the isomerization and blocks Ca^{2+}-deocclusion/release ($E2PCa_2 \rightarrow E2P + 2Ca^{2+}$) (14). Thus elongating the A/M1'-linker stabilized the normally transient intermediate state $E2PCa_2$ (*i.e.* ADP-insensitive EP with occluded Ca^{2+}), and showed that the length of this linker is critical for the structural changes that occur during $E1PCa_2 \rightarrow E2PCa_2 \rightarrow E2P + 2Ca^{2+}$ and subsequent $E2P$ hydrolysis (14, 26).

We have recently developed an $E1Ca_2 \cdot BeF_3^-$ complex as a stable analog of $E1PCa_2 \cdot Mg$

($E1PCa_2$ with bound Mg^{2+} at the catalytic site) (27). Structural analysis of the analog and intermediate states suggests that formation of native $E1PCa_2 \cdot Mg$ results in structural changes in the cytoplasmic and transmembrane domains due to configurational and ligational changes of the phosphate moiety (27). The Mg^{2+} bound at the catalytic site contributes to these structural changes (27). In fact, Ca^{2+} could not substitute for Mg^{2+} for formation of $E1Ca_2 \cdot BeF_3^-$, and an attempt to substitute Ca^{2+} for Mg^{2+} destroyed the complex (27). It is well known that Ca^{2+} substitution of Mg^{2+} at the catalytic site markedly retards $E1PCa_2 \cdot Ca$ isomerization (28, 29), a step which includes rotation of the A domain.

Further understanding of the mechanism of *E*P processing via the transient $E2PCa_2$ and of the critical roles of the A/M1'-linker and catalytic Mg^{2+} requires detailed characterization of the development of $E2PCa_2$ and of factors contributing to its possible stabilization. A great advance would be the finding of an analog stable enough for crystallographic studies.

In this study, we employed the mutant 4Gi-46/47 in which the A/M1'-linker is elongated by four glycine insertions at Gly^{46}/Lys^{47} (14), and explored formation of a stable structural analog of $E2PCa_2$ using various configurational analogs of phosphate ($BeF_x/AlF_x/MgF_x$) and catalytic cations ($Mg^{2+}/Mn^{2+}/Ca^{2+}$). We found that BeF_x is uniquely efficacious and that both mutant $E1Ca_2 \cdot BeF_3^-$ and mutant $E2 \cdot BeF_3^-$ are capable of producing mutant $E2Ca_2 \cdot BeF_x$, most probably $E2Ca_2 \cdot BeF_3^-$, and that Ca^{2+} can replace the catalytic Mg^{2+} when coming from the former species. The mutant complex $E2Ca_2 \cdot BeF_3^-$ is extremely stable even at 25 °C.

EXPERIMENTAL PROCEDURES

Mutagenesis and Expression — The pMT2 expression vector (30) carrying the mutant rabbit SERCA1a cDNA with four glycine residues inserted between Gly^{46} and Lys^{47} (4Gi-46/47) was constructed as described previously (14). Transfection of pMT2 DNA into COS-1 cells and preparation of microsomes from the cells were performed as described previously (31). The amount of expressed SERCA1a was quantified by a sandwich enzyme-linked immunosorbent assay (32). Expression levels of wild-type SERCA1a and the mutants were 2-3% of total microsomal proteins.

Metal Fluoride Treatment — Microsomes expressing the wild type or 4Gi-46/47 were treated at 25 °C for 30 min with BeF_x, AlF_x, and MgF_4^{2-} as described previously (14, 23-25, 27, 33-36) and under figure legends in detail.

Formation of EP— Phosphorylation of SERCA1a in microsomes with [γ-^{32}P]ATP was performed under conditions described in the legends to figures. The reactions were quenched with ice-cold trichloroacetic acid containing P_i. Precipitated proteins were separated by 5% SDS-PAGE at pH 6.0 according to Weber and Osborn (37). The radioactivity associated with the separated Ca^{2+}-ATPase was quantified by digital autoradiography as described (38).

Ca^{2+} Occlusion in SERCA1a — Microsomes treated with metal fluoride were diluted with "washing solution" containing excess EGTA and then immediately filtered through a 0.45-μm nitrocellulose membrane filter (Millipore). The filter was washed extensively with the washing solution, and $^{45}Ca^{2+}$ remaining on the filter was quantified. The amount of Ca^{2+} specifically bound to the transport sites of *E*P in the expressed SERCA1a was obtained by subtracting the amount of nonspecific Ca^{2+}-binding, which was determined as described in the legends to the figure. The Ca^{2+} occluded/mg of expressed SERCA1a protein was calculated from the amount of expressed SERCA1a and the amount of occluded Ca^{2+}.

Limited Proteolysis and Western Blot Analysis — Major intermediates of the Ca^{2+}-ATPase and their stable analogs were produced and subjected to structural analysis by limited proteolysis with trypsin and proteinase K (prtK) as described in the legends to the figure. Proteolysis was terminated by 2.5% (v/v) trichloroacetic acid. The digests were subjected to SDS-PAGE (39) followed by Western blot analysis with IIH11 monoclonal antibody to the rabbit SERCA1a (Affinity Bioreagents), which recognizes an epitope between Ala^{199}-Arg^{505}, as described (14).

Miscellaneous — Protein concentrations were determined by the method of Lowry *et al*. (40) with bovine serum albumin as a standard. Data were analyzed by nonlinear regression using the program Origin (Microcal Software, Inc., Northampton, MA). Three dimensional models of the enzyme were reproduced by the program VMD (41).

RESULTS

Inhibition of EP Formation by Metal

Fluoride — The $E1Ca_2$ state of wild type and mutant 4Gi-46/47 SERCA1a in 10 μM Ca^{2+} was treated with BeF_x or AlF_x and functionally analyzed. The ability to form EP from ATP (Fig. 3*A*, *C*) and from P_i (data not shown) is almost completely lost in the presence of 15 mM Mg^{2+} but not in its absence. EP formation is not inhibited when F^--treatment in 15 mM Mg^{2+} is made without Be^{2+} or Al^{3+}. The results show that the $E1Ca_2$ state of the mutant as well as of wild type forms stable complexes with BeF_x and AlF_x in the presence of Mg^{2+}, but not with MgF_x.

When the $E2$ state of wild type and mutant 4Gi-46/47 in the absence of Ca^{2+} was treated with BeF_x, AlF_x, and MgF_x (in the absence of Be^{2+} and Al^{3+}), the complexes $E2{\cdot}BeF_3^-$, $E2{\cdot}AlF_4^-$, $E2{\cdot}MgF_4^{2-}$, respectively are produced (14, 25) and EP formation from ATP (Fig. 3*B*, *D*, *open bars*) and from P_i (data not shown) is almost completely inhibited. These complexes were then treated with 10 mM Ca^{2+} for 1 h in the presence of Ca^{2+} ionophore A23187 (*black bars* in Fig. 3*B*, *D*). In the case of wild type, the ability to form EP is restored, consistent with the previous observation (25, 36) that a high concentration of Ca^{2+} in the presence of A23187 restores Ca^{2+}-ATPase activity by destroying the complexes and converting the enzyme to $E1Ca_2$. In mutant 4Gi-46/47, the Ca^{2+}-induced restoration of EP formation is observed with $E2{\cdot}MgF_4^{2-}$ and $E2{\cdot}AlF_4^-$, but not at all with $E2{\cdot}BeF_3^-$. $E2{\cdot}BeF_3^-$ of the mutant is thus resistant to Ca^{2+}. We previously found (14) that the transient intermediate $E2PCa_2$ is produced and trapped in the mutant in the reverse direction of the pump cycle from $E2$P by Ca^{2+} binding from the lumenal side, as well as in the forward direction from $E1Ca_2$ through ATP-induced phosphorylation. Therefore, the complex produced in the mutant with BeF_x is likely $E2Ca_2{\cdot}BeF_3^-$, an analog of $E2PCa_2$ (as is in fact shown later in the Ca^{2+}-binding and structural analyses in Fig. 8 and supplemental Figs. S3 and S4).

Kinetic Analysis of BeF_x-induced Complex Formation — The $E1Ca_2$ state of mutant 4Gi-46/47 was treated with various concentrations of Be^{2+} and 1 mM F^- in 10 μM Ca^{2+} and 15 mM Mg^{2+} and the resulting species analyzed (Fig. 4*A*). The presence of both Be^{2+} and F^- (BeF_x) but not F^- without Be^{2+} or Be^{2+} (20 μM) without F^- inhibits EP formation. The time courses of BeF_x-induced inhibition follow first order kinetics. A plot of the inhibition rate constants versus Be^{2+} (BeF_x) concentration is a straight line with no evidence of saturation within the experimental range, indicating that BeF_x binding is the rate-determining step in the inhibition process (Fig. 4*B*). BeF_x inhibits wild type at nearly the same rate as it does the mutant as seen at a representative 20 μM Be^{2+} with 1 mM F^-.

In Fig. 5, the mutant $E1Ca_2$ state in 10 μM Ca^{2+} was incubated with BeF_x at various Mg^{2+} concentrations, and the level of inhibition of EP formation determined. BeF_x-induced inhibition is markedly accelerated with increasing Mg^{2+}, giving a $K_{0.5}$ value of 4.9 mM. The observed apparent Mg^{2+} affinity is consistent with those values obtained through phosphorylation of native Ca^{2+}-ATPase (42-47) and for the formation of $E1Ca_2{\cdot}BeF_3^-$ ($E1PCa_2{\cdot}$Mg analog) (27), *i.e.* the Mg^{2+} binding affinity at the catalytic Mg^{2+} site (site I composed of Asp^{351}/Thr^{353}/Asp^{703} and the phosphate moiety (BeF_3^-)). Therefore, Mg^{2+} binding at site I is likely a prerequisite for BeF_x binding and complex formation.

In Figs. 6 and 7, we further observed that the BeF_x-induced complex formation from $E1Ca_2$ in the mutant occurs with Mn^{2+} or Ca^{2+} in place of Mg^{2+}. The $K_{0.5}$ values are 1.4 mM for Mn^{2+} and 0.76 mM for Ca^{2+} (supplemental Figs. S1 and S2), and are consistent with such values for binding to the catalytic Mg^{2+} site (46, 48). In wild type, the BeF_x-induced $E1Ca_2{\cdot}BeF_3^-$ formation which inhibits EP formation occurs with Mn^{2+} but not with 10 mM Ca^{2+} in place of Mg^{2+} (Figs. 6 and 7). Thus the complex formed from $E1Ca_2$ with BeF_x in the mutant 4Gi-46/47 (*i.e.* $E2Ca_2{\cdot}BeF_3^-$) is distinct from $E1Ca_2{\cdot}BeF_3^-$ of wild type.

Interestingly, the Hill coefficient for the Mg^{2+}, as well as Mn^{2+} and Ca^{2+}, dependence for complex formation with BeF_x ($E2Ca_2{\cdot}BeF_3^-$) in the mutant is nearly 2 (Fig. 5 and supplemental Figs. S1 and S2), suggesting the involvement of more than one metal ion. This is in contrast to the value 1 for $E1Ca_2{\cdot}BeF_3^-$ formation with Mg^{2+} and Mn^{2+} in wild type (see Supplemental Fig. 1 in Ref. 27).

AlF_x produces the complex with the $E1Ca_2$ state of the mutant 4Gi-46/47 as well as of wild type ($E1Ca_2{\cdot}AlF_x$) with Mg^{2+} and Mn^{2+} but not with Ca^{2+} at the catalytic Mg^{2+} site (Figs. 3, 6, and 7). Therefore in the mutant, the complex with AlF_x ($E1Ca_2{\cdot}AlF_x$) is distinct from that with BeF_x ($E2Ca_2{\cdot}BeF_3^-$) with respect to the strict preference of the divalent cation at the catalytic Mg^{2+} site.

Ca^{2+} Occlusion in the Mutant Complexed with BeF_x — In Fig. 8*A*, the $E1Ca_2$ state of the mutant 4Gi-46/47 in 10 μM $^{45}Ca^{2+}$ and 15 mM Mg^{2+} was complexed with BeF_x at a low

concentration of Be^{2+} (1 μM) with 1 mM F^- in order to slow complex formation. The amount of occluded $^{45}Ca^{2+}$ was determined at various periods by membrane filtration with extensive washing with a solution containing excess EGTA and A23187. The loss of *E*P forming ability with ATP decreases reciprocally and linearly with an increase in the amount of occluded Ca^{2+} (see *inset*). The amount of occluded $^{45}Ca^{2+}$ at the intercept of the abscissa, *i.e.* when all the ATPases are complexed with BeF_x, is 8.4 nmol/mg of expressed SERCA1a mutant protein. The stoichiometry of the occluded Ca^{2+} is nearly 2 per phosphorylation site, which is 4.3 nmol/mg as determined from the intercept on the ordinate. Therefore the complex formed with BeF_x has two occluded Ca^{2+}. When the mutant was incubated for 15 min with BeF_x and 1.5 mM Mn^{2+} in place of Mg^{2+} under otherwise identical conditions, *E*P formation is completely inhibited and the amount of occluded $^{45}Ca^{2+}$ is 8.3 nmol/mg of expressed SERCA1a mutant protein, giving a stoichiometry of 2 per phosphorylation site (data not shown).

In Fig. 8*B*, we examined whether the complex $E2Ca_2{\cdot}BeF_3^-$ can be produced from $E2{\cdot}BeF_3^-$ by lumenal Ca^{2+} binding, mimicking the reverse conversion $E2P + 2Ca^{2+} \rightarrow E2PCa_2$ (14). $E2{\cdot}BeF_3^-$ was first formed in the mutant in the absence of Ca^{2+}, and then incubated for 1 min at 25 °C with various concentrations of $^{45}Ca^{2+}$ in the presence of Ca^{2+} ionophore A23187. The amount of occluded $^{45}Ca^{2+}$ was determined after a large dilution followed by filtration and extensive EGTA washing. The maximum amount of occluded $^{45}Ca^{2+}$ is 7.7 nmol/mg of mutant SERCA1a protein and 1.8 times that of the phosphorylation site (4.3 nmol/mg), giving a stoichiometry of nearly 2. Thus mutant $E2Ca_2{\cdot}BeF_3^-$ is produced from mutant $E2{\cdot}BeF_3^-$ by the addition of Ca^{2+} in the presence of A23187.

$K_{0.5}$ and the Hill coefficient observed in Fig. 8*B* are 0.1 mM and approximately 2 respectively, *i.e.* very similar values to those observed during $E2PCa_2$ formation from *E*2P and Ca^{2+} in the mutant (14). The observed low Ca^{2+} affinity is in agreement with the wild-type property (25, 49) that $E2{\cdot}BeF_3^-$ as well as *E*2P have low affinity Ca^{2+} binding sites — the lumenally oriented transport sites. Importantly, $E2Ca_2{\cdot}BeF_3^-/E2PCa_2$ formed in the mutant (either from $E1Ca_2$ or from $E2{\cdot}BeF_3^-/E2P$) are remarkably stable and virtually not in equilibrium with $E1Ca_2{\cdot}BeF_3^-/E1PCa_2$ or $E2{\cdot}BeF_3^-/E2P$, *i.e.* their formation is almost irreversible, as shown previously (14) and in the present study. When Ca^{2+} comes from the cytoplasmic side for $E2PCa_2$ formation from $E1Ca_2$ with ATP (via $E2 \rightarrow E1Ca_2 \rightarrow E1PCa_2 \rightarrow E2PCa_2$) in the mutant, the apparent Ca^{2+} affinity is very high with $K_{0.5}$=0.14 μM (14) equal to the value for cytoplasmic Ca^{2+} binding at the transport sites in wild type. Also in the case of mutant $E2Ca_2{\cdot}BeF_3^-$ formation from $E1Ca_2$ with BeF_x in Fig. 8*A*, 10 μM Ca^{2+} is obviously enough to saturate (even 1 μM Ca^{2+} saturates (data not shown)), suggesting a similar high Ca^{2+} affinity as in $E2PCa_2$ formation from $E1 + 2Ca^{2+}$.

Structures of Complexes Formed from E1Ca$_2$ with Metal Fluoride — During the Ca^{2+} transport cycle, the A, P, and N domains move and reorganize substantially. These changes can be monitored by proteolytic patterns and resistance against trypsin and proteinase K (prtK) (23, 24). Therefore, we applied proteolytic analyses to mutant $E2Ca_2{\cdot}BeF_3^-$ in order to reveal the position of the domains and to establish whether it is a true structural $E2PCa_2$ analog (supplemental Figs. S3 and S4, and Tables S1 and S2 with additional Refs. 54 and 55). All the various major intermediates and their analogs were formed from $E1Ca_2$ in the mutant and wild type, and then subjected to proteolyses. The results show that mutant $E2Ca_2{\cdot}BeF_3^-$ has the same structure as that of mutant $E2PCa_2$, and that this structural state is intermediate between wild type $E1PCa_2$ (wild type $E1Ca_2{\cdot}BeF_3^-$) and Ca^{2+}-free *E*2P (wild type as well as mutant $E2{\cdot}BeF_3^-$) as described below.

In mutant $E2Ca_2{\cdot}BeF_3^-$ and in mutant $E2PCa_2$, the T2 site Arg^{198} on the Val^{200} loop is completely resistant to trypsin, as in wild type *E*2P ($E2{\cdot}BeF_3^-$), showing that the A domain has rotated from its position in $E1PCa_2$ ($E1Ca_2{\cdot}BeF_3^-$ of wild type) and is associated with the P domain at Arg^{198} of the Val^{200} loop.

In both wild type $E1Ca_2{\cdot}BeF_3^-$ ($E1PCa_2$) and wild type and mutant $E2{\cdot}BeF_3^-$ (*E*2P), Leu^{119} on the upper portion of M2 is completely resistant to prtK attack and thus sterically protected, as found previously (25, 27; see detailed description and reasons for protection in supplemental Fig. S5 with an additional Ref. 56). By contrast, in mutant $E2Ca_2{\cdot}BeF_3^-$ and mutant $E2PCa_2$, the prtK-site Leu^{119} is rapidly cleaved and thus exposed. Evidently, Leu^{119}/Tyr^{122} on M2 in mutant $E2Ca_2{\cdot}BeF_3^-$ and mutant $E2PCa_2$ have moved from their hidden position in $E1PCa_2$ ($E1Ca_2{\cdot}BeF_3^-$) but are not yet buried again through interaction with the A and P domains as in *E*2P ($E2{\cdot}BeF_3^-$) – suggesting an intermediate

structure. The results also reveal how critical the native length of the A/M1'-linker is for moving M2 and the A and P domains to realize the Ca^{2+}-free state *E*2P (*E*2·BeF_3^-).

The proteolyses also reveal that wild type and mutant *E*1Ca_2·AlF_x are not structurally similar to wild type *E*1Ca_2·BeF_3^- (*E*1PCa_2) and mutant *E*2Ca_2·BeF_3^- (*E*2PCa_2). Interestingly, the rate of cleavage at the T2 site of mutant *E*1Ca_2·AlF_x is intermediate between that of wild-type transition state (*E*1Ca_2·AlF_x/*E*1Ca_2·AlF_4^-·ADP) and that of *E*1PCa_2 product state (*E*1Ca_2·BeF_3^-), suggesting that the structure is also intermediate. Thus elongation of the A/M1'-linker brought the *E*1Ca_2·AlF_x structure closer to that of wild type *E*1Ca_2·BeF_3^-. Only BeF_x, and not AlF_x, produces a species analogous to the *E*2PCa_2 structural state (*E*2Ca_2·BeF_3^- via *E*1Ca_2·BeF_3^-). This means that the phosphorylation reaction must have passed through the transition state in order to progress to the isomerization step.

In the mutant and wild type, the prtK-site Thr^{242} on the A/M3-linker is completely resistant in all the states *E*1Ca_2·AlF_4^-·ADP/*E*1Ca_2·AlF_x, *E*1Ca_2·BeF_3^- (*E*1PCa_2), *E*2Ca_2·BeF_3^- and *E*2PCa_2, and *E*2·BeF_3^-/*E*2·AlF_4^-/*E*2·MgF_4^{2-} (as shown previously with SR Ca^{2+}-ATPase (23, 24)). The result indicates that in both mutant and wild type, the A/M3-linker is strained by the A-domain rotation perpendicular to the membrane plane upon *E*1PCa_2 formation from *E*1Ca_2 and remains taut during *E*P processing.

E2Ca₂·BeF₃⁻ Formation from E2·BeF₃⁻ by Lumenal Ca^{2+} Binding — The Ca^{2+}-free complexes *E*2·BeF_3^-, *E*2·AlF_4^-, and *E*2·MgF_4^{2-} (the analogs of the *E*2P ground state, transition state, and product complex of *E*2P hydrolysis, respectively (25)) were first formed in mutant 4Gi-46/47 and wild type with Mg^{2+} bound at the catalytic site and subsequent proteolyses performed with and without a 10 mM Ca^{2+} treatment in the presence of ionophore A23187 (supplemental Fig. S4 and Table S2). Under these conditions Ca^{2+}-treated mutant *E*2·BeF_3^- exhibits complete resistance at the tryptic T2 site Arg^{198} and a fairly rapid prtK-cleavage at Leu^{119} on the top of M2, exactly as in mutant *E*2PCa_2 and *E*2Ca_2·BeF_3^- produced from *E*1Ca_2. These results agree with those in Fig. 3*D* where it is found that the ability to form *E*P is not restored by Ca^{2+} treatment of *E*2·BeF_3^-. Thus, *E*2Ca_2·BeF_3^- as the *E*2PCa_2 analog is produced from both *E*2·BeF_3^- and from *E*1Ca_2 (mimicking lumenal Ca^{2+} binding to *E*2P in the reverse direction of the pump cycle and the forward ATP-induced *E*P formation and isomerization, respectively). On the other hand, mutant and wild-type complexes *E*2·AlF_4^- and *E*2·MgF_4^{2-}, and wild-type *E*2·BeF_3^- are destroyed by Ca^{2+} treatment as found previously with SR Ca^{2+}-ATPase (25, 27).

Stability of Complex E2Ca₂·BeF₃⁻ — In Fig. 9, *E*2Ca_2·BeF_3^- was first produced from mutant *E*1Ca_2 with BeF_x in 50 μM $^{45}Ca^{2+}$ and 15 mM Mg^{2+}, then further incubated at 25 °C in the presence of these ligands and the amount of occluded $^{45}Ca^{2+}$ determined. The results show that the complex *E*2Ca_2·BeF_3^- of the mutant is perfectly stable even after one week. Proteolysis confirms that the structure remains unchanged during the incubation (data not shown). The stability of the complex was further tested by diluting into an EGTA-containing solution without BeF_x, and the incubation continued at 25 °C (see *inset*). Ca^{2+} is slowly released with a rate constant of 7.0 h^{-1}. Addition of thapsigargin (TG) to the diluent only doubles the rate of release, indicating that the transmembrane domain is fairly resistant to TG-induced structural perturbation. These decay rates are very similar to those of mutant *E*2PCa_2 without and with TG addition, 9.7 and 27.3 h^{-1}, respectively (14). Thus in this respect also, mutant *E*2Ca_2·BeF_3^- is analogous to mutant *E*2PCa_2.

DISCUSSION

Mutant E2Ca₂·BeF₃⁻ as an Analog of Native Transient State E2PCa₂ — Using our elongated A/M1'-linker mutant, we have developed the complex *E*2Ca_2·BeF_x, most probably *E*2Ca_2·BeF_3^-, as a stable structural analog of the native transient state *E*2PCa_2 (ADP-insensitive *E*P with two Ca^{2+} at the transport sites), an intermediate in *E*P isomerization and Ca^{2+}-deocclusion/release. The complex *E*2Ca_2·BeF_3^- has two occluded Ca^{2+}, and is produced from both mutant *E*1Ca_2 and mutant *E*2·BeF_3^-, mimicking native *E*2PCa_2 formation from *E*1Ca_2 following ATP-induced forward phosphorylation via *E*1PCa_2 isomerization and in the reverse direction from *E*2P following lumenal Ca^{2+} binding. Mutant *E*2Ca_2·BeF_3^- formation requires Mg^{2+} at the catalytic site as in native ATP- and P_i-induced *E*P formation. The disposition of the cytoplasmic domains in mutant *E*2Ca_2·BeF_3^- is equivalent to that in *E*2PCa_2 trapped with the mutant, and intermediate between native *E*1PCa_2·Mg (*E*1Ca_2·BeF_3^- of wild type) and native *E*2P·Mg

($E2{\cdot}BeF_3^-$ of wild type and mutant). All these properties of mutant $E2Ca_2{\cdot}BeF_3^-$ meet the requirements of a native $E2PCa_2$ analog.

Importantly, AlF_x and MgF_x are not able to produce this $E2PCa_2$ analog either from mutant $E1Ca_2$ or from mutant $E2{\cdot}AlF_4^-$ and $E2{\cdot}MgF_4^{2-}$. Thus BeF_x is unique in this regard. The coordination chemistry of the beryllium in BeF_x (BeF_3^-) allows it to directly ligate the aspartyl oxygen, thereby producing the same tetrahedral geometry as the covalent Asp^{351}-acylphosphate, as seen in the atomic structure of the $E2P$ ground state analog $E2{\cdot}BeF_3^-$ (21, 22). On the other hand, AlF_x (AlF_3 or AlF_4^-) mimics the transition state of phosphorylation and dephosphorylation as seen in structures $E1Ca_2{\cdot}AlF_4^-{\cdot}$ADP and $E2{\cdot}AlF_4^-$ (17, 19, 22). MgF_4^{2-} mimics P_i in the product complex $E2{\cdot}P_i$ following $E2P$ hydrolysis as seen in structure $E2{\cdot}MgF_4^{2-}$ (19). Our results taken together with the coordination chemistry show that the structural changes for EP isomerization and Ca^{2+}-deocclusion/release in the forward and reverse reactions are strictly coupled with the particular configuration of the acylphosphate following formation of the covalent bond within the catalytic site. The product $E1PCa_2$ state and the $E2P$ ground state are ready for the changes, but the transition-state structures are not.

Roles of A/M1'-linker and Structural Changes during EP Formation and Processing — The transient $E2PCa_2$ state formed during EP processing and its analog $E2Ca_2{\cdot}BeF_3^-$ were trapped and stabilized by elongation of the A/M1'-linker. As revealed by the proteolyses, in mutant $E2Ca_2{\cdot}BeF_3^-$ and mutant $E2PCa_2$, the A domain has already rotated parallel to membrane from its position in $E1Ca_2{\cdot}BeF_3^-$ ($E1PCa_2{\cdot}$Mg) and has associated with the P domain at the Val^{200} loop. Because mutant $E2PCa_2$ is ADP-insensitive (14), the outermost loop $TGES^{184}$ of the A domain is most probably docked onto the Asp^{351}-region thereby blocking ADP access to the Asp^{351}-acylphosphate (19). Thus in mutant $E2Ca_2{\cdot}BeF_3^-$ and mutant $E2PCa_2$, the A domain is positioned above the P domain. On the other hand, the proteolyses also show that the spatial relationship of the top part of M2 (Leu^{119}/Tyr^{122}) with the P and A domains in mutant $E2Ca_2{\cdot}BeF_3^-$ (equivalent to native $E2PCa_2{\cdot}$Mg) is intermediate between those of the wild type $E1Ca_2{\cdot}BeF_3^-$ (native $E1PCa_2{\cdot}$Mg) and the wild type and mutant $E2{\cdot}BeF_3^-$ (native $E2P{\cdot}$Mg). Thus Leu^{119} (the prtK site) on the top part of M2 has broken its van der Waals contact with upper M4 seen in $E1PCa_2$, but has not yet reached the P and A domains to form their interaction network at Leu^{119}/Tyr^{122}, *i.e.* the Tyr^{122}-hydrophobic cluster has not formed (see supplemental Fig. S5 for its structure). This interaction network formed from Ile^{179}/Leu^{180}/Ile^{232} of the A domain, Val^{705}/Val^{726} of the P domain, and Tyr^{122}/Leu^{119} of M2 is actually critical for the $E2P$ structure (11-13). Therefore in $E2Ca_2{\cdot}BeF_3^-$ and $E2PCa_2$ stabilized by elongation of the A/M1'-linker, the inclining motions of domains and helix are not yet advanced enough to reach the $E2P$ structure.

Deletion of any single residue in the A/M1'-linker, *i.e.* shortening it, completely blocks $E1PCa_2$ isomerization to $E2PCa_2$ (26). By contrast, its elongation markedly accelerates the isomerization and greatly stabilizes $E2PCa_2$ blocking Ca^{2+}-deocclusion/release from this transient state (14). These findings suggest that formation of the transient $E2PCa_2$ state (mutant $E2Ca_2{\cdot}BeF_3^-$) from $E1PCa_2$ ($E1Ca_2{\cdot}BeF_3^-$), strains the A/M1'-linker with the wild-type/native length due to rotation and positioning of the A domain above the P domain, which in turn causes further movements of the A and P domains facilitating Ca^{2+}-deocclusion/release (14) (see the cartoon model in supplemental Fig. S6). The A and P domains incline more, as will M1/M2 and M4/M5 connected with these domains, favoring release of the Ca^{2+}. This view agrees with the structural changes required for Ca^{2+} release described by Toyoshima *et al.* (19): the bending and movement of M4/M5 by inclination of the P domain is predicted to destroy the Ca^{2+} binding sites, and the inclination of M2 and M1 (as a V-shaped rigid body) will push the lower part of M4 via M1 and open the lumenal gate.

These domain and segmental motions associated with Ca^{2+} release will establish the interaction network at Leu^{119}/Tyr^{122}, the Tyr^{122}-hydrophobic cluster, and stabilize the $E2P$ structure with the lumenal gate open (11-13). The position of the two A-P domain interaction networks, with Leu^{119}/Tyr^{122} at the lower part and Val^{200} loop on the upper part of the interface, seems particularly appropriate to stabilize the inclined A and P domains and helices and therefore the gate in an open state.

These cluster formations are also critical for producing the $E2P$ catalytic site with hydrolytic ability (11-13). Therefore in this mechanism, $E2P$ hydrolysis can only occur after Ca^{2+} release, ensuring energy coupling. The relative stability of native $E2P$ may

function as a brake to allow enough time for releasing Ca^{2+} and for refining the catalytic site for subsequent hydrolysis, *e.g.* appropriate positioning of $TGES^{184}$ and Glu^{183}-coordinated attacking water molecule.

Ca^{2+} Substitution of Mg^{2+} at the Catalytic Site — In the elongated A/M1'-linker mutant, Ca^{2+} as well as Mg^{2+} bound at the catalytic Mg^{2+} site is able to produce $E2Ca_2{\cdot}BeF_3^-$ from $E1Ca_2$ via $E1Ca_2{\cdot}BeF_3^-$. This binding of Ca^{2+} is also found when mutant $E2PCa_2$ is formed from CaATP in the absence of Mg^{2+} (14). This is in sharp contrast to the situation in wild type, where Ca^{2+} cannot substitute for Mg^{2+} at the catalytic site for $E1Ca_2{\cdot}BeF_3^-$ formation. An attempt to substitute Ca^{2+} for Mg^{2+} actually destroys wild type $E1Ca_2{\cdot}BeF_3^-$ (27). The extremely rapid isomerization of *E*P with bound Ca^{2+} at the Mg^{2+} site in the elongated A/M1'-linker mutant ($E1PCa_2{\cdot}Ca \rightarrow E2PCa_2{\cdot}Ca$) is again very different to the markedly retarded $E1PCa_2{\cdot}Ca$ isomerization in wild type (14). The atomic structures provide insights into why elongation of the linker allows Ca^{2+} to replace Mg^{2+} at the catalytic site.

In the atomic structures of $E1Ca_2{\cdot}$CaAMPPCP and $E1Ca_2{\cdot}AlF_4^-{\cdot}$ADP described by Toyoshima *et al*. (18, 19), Mg^{2+}- or Ca^{2+}-ligation at the catalytic Mg^{2+} site I (Asp^{351}/Thr^{353}/Asp^{703} of the P domain and the phosphate moiety (or its analog), see Fig. 2) induces the P domain to bend and thereby the A domain to rotate upwards, perpendicular to the membrane plane (see Figures 4 and 5 in Ref. 18, and the cartoon in supplemental Fig. S6). This A-domain rotation raises its junctions with the A/M1'-linker and the A/M3-linker. The strain imposed on the A/M3-linker in $E1PCa_2$ probably drives the large horizontal rotation of the A domain during $E1PCa_2$ to *E*2P isomerization (18, 19, 50, 51). In the stringent coordination chemistry, the ligation length is shorter in Mg^{2+} than in Ca^{2+} typically by 0.2 Å (*e.g.* 2.1 versus 2.3 Å (52, 53)). Therefore Mg^{2+} ligation probably induces more P-domain bending and in consequence more upward swinging of the A domain leading to a stronger pull from the A/M3-linker to effect the horizontal rotation of the A domain (27). This is substantiated by the finding that in wild type $E1PCa_2{\cdot}Mg$ is rapidly isomerized whereas in $E1PCa_2{\cdot}Ca$ it is markedly retarded (28, 29).

The observed formation of $E2Ca_2{\cdot}BeF_3^-$ and $E2PCa_2$ (via very rapid $E1PCa_2$ isomerization) from mutant $E1Ca_2$ with Ca^{2+} or Mg^{2+} at the catalytic Mg^{2+} site shows that the poor Ca^{2+}-effect on the A-domain's upward rotation and subsequent horizontal rotation is relieved by elongation of the A/M1'-linker. Note again that the A-domain's junction with the A/M1'-linker is raised by the upward movement of the A domain. It is therefore likely that in wild type, the A/M1'-linker is strained to some extent by this movement of the A domain on formation of $E1PCa_2$. This possible strain is evidently not deleterious for wild type, but it becomes a serious energy barrier when the A/M1'-linker is shortened by deletion of any single residue since the deletions completely block $E1PCa_2$ to $E2PCa_2$ isomerization (26). Strain in the wild-type A/M1'-linker in $E1PCa_2$ is likely to be important as a build up to generating stronger strain during $E1PCa_2$ to $E2PCa_2$ isomerization. Thus, the strain of the A/M1'-linker seems to be imposed increasingly during $E1PCa_2$ formation and the subsequent isomerization to $E2PCa_2$, and this energy finally could be used for inducing structural changes for Ca^{2+}-deocclusion and release.

$E1Ca_2{\cdot}AlF_x$ Formed from $E1Ca_2$ in the Elongated A/M1'-linker Mutant — The proteolytic analyses reveal that in wild type, organization of the cytoplasmic domains of the transition state analog $E1Ca_2{\cdot}AlF_x$ is identical to that of $E1Ca_2{\cdot}AlF_4^-{\cdot}$ADP, and has obviously not yet reached the product $E1PCa_2$ state $E1Ca_2{\cdot}BeF_3^-$. Namely, during the reaction $E1Ca_2{\cdot}AlF_4^-{\cdot}ADP/E1Ca_2{\cdot}AlF_x \rightarrow E1Ca_2{\cdot}BeF_3^-$, the A domain rotates partially in a horizontal direction and to come close to the P domain at tryptic T2 site Arg^{198}, but is not completely engaged, so that it cannot produce the $E2Ca_2{\cdot}BeF_3^-$ and $E2{\cdot}BeF_3^-$ states, (Ref. 27, and see the cartoon in supplemental Fig. S6). On the other hand, in the elongated A/M1'-linker mutant, the structure of $E1Ca_2{\cdot}AlF_x$ is intermediate between those of $E1Ca_2{\cdot}AlF_4^-{\cdot}$ADP and $E1Ca_2{\cdot}BeF_3^-$ of wild type as judged from the intermediate tryptic cleavage rate at Arg^{198}. Thus elongation of the A/M1'-linker partly relieves barriers to A-domain rotation, bringing the structure of $E1Ca_2{\cdot}AlF_x$ closer to that of $E1Ca_2{\cdot}BeF_3^-$. The finding agrees with our above postulate that the A/M1'-linker is strained by the A-domain's upward movement during $E1PCa_2$ ($E1Ca_2{\cdot}BeF_3^-$) formation from the transition state ($E1Ca_2{\cdot}AlF_x$). In fact, since the length of the Asp^{351} O-phosphate bond in the transition state (as mimicked by AlF_x) is obviously longer than that of the covalent acylphosphate bond (as mimicked by BeF_3^-), the transition state (AlF_x) must exhibit less

P-domain bending.

Lumenal Ca^{2+}-induced $E2Ca_2{\cdot}BeF_3^-$ Formation from $E2{\cdot}BeF_3^-$ — The observed reverse formation of $E2Ca_2{\cdot}BeF_3^-$ (native $E2PCa_2$) from mutant $E2{\cdot}BeF_3^-$ ($E2P$) through Ca^{2+} binding from the lumen shows that the lumenal gate (Ca^{2+} releasing pathway) is open in $E2{\cdot}BeF_3^-$ ($E2P$ ground state immediately before Ca^{2+} binding). This is in contrast to the closed gate in $E2{\cdot}AlF_4^-$ and $E2{\cdot}MgF_4^{2-}$ (25). Thus, lumenal gating is strictly coupled with the configurational change in the phosphate during $E2P$ hydrolysis, thereby avoiding possible Ca^{2+} leakage (25). Note that in wild type, $E2{\cdot}BeF_3^-$ (open lumenal gate) formed with Mg^{2+} is converted to $E1Ca_2$ + BeF_x by Ca^{2+}, because cycle reversal and subsequent Ca^{2+} substitution of Mg^{2+} at the catalytic site destabilizes $E1Ca_2{\cdot}BeF_3^-$ as previously demonstrated (27). $E2{\cdot}AlF_4^-$ and $E2{\cdot}MgF_4^{2-}$ (gates closed) in wild type and mutant were also decomplexed to $E1Ca_2$ by Ca^{2+}, but probably by the high Ca^{2+} concentration disrupting the lumenal and transmembrane regions, thereby destabilizing AlF_4^-- and MgF_4^{2-}-ligation at the catalytic site.

Mg^{2+}-dependence of $E2Ca_2{\cdot}BeF_3^-$ Formation from $E1Ca_2$ — The Mg^{2+}, as well as Mn^{2+} or Ca^{2+}, dependence of $E2Ca_2{\cdot}BeF_3^-$ formation from mutant $E1Ca_2$ (Fig. 5 and supplemental Figs. S1 and S2) exhibited a Hill coefficient of 2, which is in contrast to the value of 1 for wild type $E1Ca_2{\cdot}BeF_3^-$ formation from $E1Ca_2$ (27). The results suggest that one or more Mg^{2+} besides the one at the catalytic Mg^{2+} site I is involved cooperatively in the $E2Ca_2{\cdot}BeF_3^-$ formation from $E1Ca_2$. In the atomic structures of $E1Ca_2{\cdot}$CaAMPPCP and $E1Ca_2{\cdot}AlF_4^-{\cdot}$ADP, only one Mg^{2+} (or Ca^{2+}) at site I is seen (in addition to the one coordinated with the nucleotide, which was predicted to aid phosphoryl transfer). Also in the structures of $E2{\cdot}BeF_3^-$, $E2{\cdot}AlF_4^-$, and $E2{\cdot}MgF_4^{2-}$, only one Mg^{2+} is seen (at site I). Therefore, in $E2Ca_2{\cdot}BeF_3^-$ ($E2PCa_2$) formation a second (or more) Mg^{2+} may possibly be required only transiently and, together with the catalytic ion, aids the motions of N, P, and A domains and their gathering during the $E1PCa_2$ isomerization to $E2PCa_2$.

In summary, our previous (14, 26) and present studies show that the A/M1'-linker should be appropriately long for the $E1PCa_2$ to $E2PCa_2$ isomerization, then short enough for the Ca^{2+}-deocclusion/release from $E2PCa_2$, and again appropriately long for $E2P$ hydrolysis. Thus the length of the A/M1'-linker in wild type is naturally designed to induce successive structural changes and motions of the cytoplasmic and transmembrane domains for these processes. These functions of the A/M1'-linker act in concert with the changing configuration of the phosphate and catalytic Mg^{2+}, the Asp^{351}-phosphate bond length and strength being critical in the formation of $E2PCa_2$, a species poised to deliver Ca^{2+} to the lumen. The stable analogs, $E1Ca_2{\cdot}BeF_3^-$ (27) and $E2Ca_2{\cdot}BeF_3^-$ (this study) with bound Mg^{2+} could be critically important for obtaining atomic models of $E1PCa_2{\cdot}Mg$ and the hitherto elusive transient $E2PCa_2{\cdot}Mg$ intermediate for further understanding of the transport mechanism.

Acknowledgments — We would like to thank Dr. David H. MacLennan, University of Toronto, for his generous gift of SERCA1a cDNA and Dr. Randal J. Kaufman, Genetics Institute, Cambridge, MA, for his generous gift of the expression vector pMT2. We are also grateful to Dr. Chikashi Toyoshima, University of Tokyo, for helpful discussions. We thank Dr. David B. McIntosh for reviewing and improving our manuscript.

REFERENCES

1. Hasselbach, W., and Makinose, M. (1961) *Biochem. Z.* **333,** 518-528
2. Ebashi, S., and Lipmann, F. (1962) *J. Cell Biol.* **14,** 389-400
3. Inesi, G., Sumbilla, C., and Kirtley, M. E. (1990) *Physiol. Rev.* **70,** 749-776
4. Møller, J. V., Juul, B., and le Maire, M. (1996) *Biochim. Biophys. Acta* **1286,** 1-51
5. MacLennan, D. H., Rice, W. J., and Green, N. M. (1997) *J. Biol. Chem.* **272,** 28815-28818
6. McIntosh, D. B. (1998) *Adv. Mol. Cell Biol.* **23A,** 33-99
7. Toyoshima, C., and Inesi, G. (2004) *Annu. Rev. Biochem.* **73,** 269-292
8. Toyoshima, C. (2008) *Arch. Biochem. Biophys.* **476,** 3-11
9. Toyoshima, C. (2009) *Biochim. Biophys. Acta* **1793,** 941-946
10. Kato, S., Kamidochi, M., Daiho, T., Yamasaki, K., Wang, G., and Suzuki, H. (2003) *J. Biol. Chem.* **278,** 9624-9629
11. Yamasaki, K., Daiho, T., Danko, S., and Suzuki, H. (2004) *J. Biol. Chem.* **279,** 2202-2210

12. Wang, G., Yamasaki, K., Daiho, T., and Suzuki, H. (2005) *J. Biol. Chem.* **280,** 26508-26516
13. Yamasaki, K., Wang, G., Daiho, T., Danko, S., and Suzuki, H. (2008) *J. Biol. Chem.* **283,** 29144-29155
14. Daiho, T., Yamasaki, K., Danko, S., and Suzuki, H. (2007) *J. Biol. Chem.* **282,** 34429-34447
15. Toyoshima, C., Nakasako, M., Nomura, H., and Ogawa, H. (2000) *Nature* **405,** 647-655
16. Toyoshima, C., and Nomura, H. (2002) *Nature* **418,** 605-611
17. Sørensen, T. L-M., Møller, J. V., and Nissen, P. (2004) *Science* **304,** 1672-1675
18. Toyoshima, C., and Mizutani, T. (2004) *Nature* **430,** 529-535
19. Toyoshima, C., Nomura, H., and Tsuda, T. (2004) *Nature* **432,** 361-368
20. Olesen, C., Sørensen, T. L.-M., Nielsen, R. C., Møller, J. V., and Nissen, P. (2004) *Science* **306,** 2251-2255
21. Toyoshima, C., Norimatsu, Y., Iwasawa, S., Tsuda, T., and Ogawa, H. (2007) *Proc. Natl. Acad. Sci. U. S. A.* **104,** 19831-19836
22. Olesen, C., Picard, M., Winther, A.-M. L., Gyrup, C., Morth, J. P., Oxvig, C., Møller, J. V., and Nissen, P. (2007) *Nature* **450**, 1036-1042.
23. Danko, S., Daiho, T., Yamasaki, K., Kamidochi, M., Suzuki, H., and Toyoshima, C. (2001) *FEBS Lett.* **489,** 277-282
24. Danko, S., Yamasaki, K., Daiho, T., Suzuki, H., and Toyoshima, C. (2001) *FEBS Lett.* **505,** 129-135
25. Danko, S., Yamasaki, K., Daiho, T., and Suzuki, H. (2004) *J. Biol. Chem.* **279,** 14991-14998
26. Daiho, T., Yamasaki, K., Wang, G., Danko, S., Iizuka, H., and Suzuki, H. (2003) *J. Biol. Chem.* **278,** 39197-39204
27. Danko, S., Daiho, T., Yamasaki, K., Liu, X., and Suzuki, H. (2009) *J. Biol. Chem.* **284,** 22722-22735
28. Shigekawa, M., Wakabayashi, S., and Nakamura, H. (1983) *J. Biol. Chem.* **258,** 8698-8707
29. Wakabayashi, S., and Shigekawa, M. (1987) *J. Biol. Chem.* **262,** 11524-11531
30. Kaufman, R. J., Davies, M. V., Pathak, V. K., and Hershey, J. W. B. (1989) *Mol. Cell. Biol.* **9,** 946–958
31. Maruyama, K., and MacLennan, D. H. (1988) *Proc. Natl. Acad. Sci. U. S. A.* **85,** 3314-3318
32. Daiho, T., Yamasaki, K., Suzuki, H., Saino, T., and Kanazawa, T. (1999) *J. Biol. Chem.* **274,** 23910-23915
33. Murphy, A. J., and Coll, R. J. (1992) *J. Biol. Chem.* **267,** 5229-5235
34. Troullier, A., Girardet, J.-L., and Dupont, Y. (1992) *J. Biol. Chem.* **267,** 22821-22829
35. Murphy, A. J., and Coll, R. J. (1993) *J. Biol. Chem.* **268,** 23307-23310
36. Kubota, T., Daiho, T., and Kanazawa, T. (1993) *Biochim. Biophys. Acta* **1163,** 131-143
37. Weber, K., and Osborn, M. (1969) *J. Biol. Chem.* **244,** 4406–4412
38. Daiho, T., Suzuki, H., Yamasaki, K., Saino, T., and Kanazawa, T. (1999) *FEBS Lett.* **444,** 54-58
39. Laemmli, U. K. (1970) *Nature* **277,** 680-685
40. Lowry, O. H., Rosebrough, N. J., Farr, A. L., and Randall, R. J. (1951) *J. Biol. Chem.* **193,** 265–275
41. Humphrey, W., Dalke, A., and Schulten, K. (1996) *J. Mol. Graphics* **14,** 33-38
42. de Meis, L., and Masuda, H. (1974) *Biochemistry* **13,** 2057-2062
43. Masuda, H., and de Meis, L. (1973) *Biochemistry* **12,** 4581-4585
44. Hasselbach, W., Fassold, E., Migala, A., and Rauch, B. (1981) *Fed. Proc.* **40,** 2657-2661
45. Gonzales, D. A., Ostuni, M. A., Lacapere, J-J., and Alonso, G. L. (2006) *Biophys. Chem.* **124,** 27-34
46. Yamada, S., and Ikemoto, N. (1980) *J. Biol. Chem.* **255,** 3108-3119
47. Kanazawa, T. (1975) *J. Biol. Chem.* **250,** 113-119
48. Ogurusu, T., Wakabayashi, S., and Shigekawa, M. (1991) *J. Biochem.* (*Tokyo*) **109,** 472-476
49. de Meis, L., and Inesi, G. (1982) *J. Biol. Chem.* **257,** 1289-1294
50. Møller, J. V., Lenoir, G., Marchand, C., Montigny, C., le Maire, M., Toyoshima, C., Juul, B. S., and Champeil, P. (2002) *J. Biol. Chem.* **277,** 38647-38659
51. Holdensen, A. N., and Andersen, J. P. (2009) *J. Biol. Chem.* **284,** 12258-12265
52. Picard, M., Jensen, A-M. L., Sørensen, T. L-M., Champeil, P., Moller, J. V., and Nissen, P. (2007) *J. Mol. Biol.* **368,** 1-7
53. Peeraer, Y., Rabijns, A., Collet, J. F., Van Schaftingen, E., and De Ranter, C. (2004) *Eur. J. Biochem*. **271,** 3421-3427

54. Juul, B., Turc, H., Durand, M.L., Gomez de Gracia, A., Denoroy, L., Møller, J. V., Champeil, P. and le Maire, M. (1995) *J. Biol. Chem.* **270,** 20123-20134
55. Lenoir, G., Picard, M., Gauron, C., Montigny, C., Le Maréchal, P., Falson, P., le Maire, M., Møller, J. V., and Champeil, P. (2004) *J. Biol. Chem.* **279,** 9156-9166
56. Seekoe, T., Peall, S., and McIntosh, D. B. (2001) *J. Biol. Chem.* **276,** 46737-46744

FOOTNOTES

*This work was supported by Grant-in-Aid for Scientific Research (C) (to T.D.) and (B) (to H.S.) from the Ministry of Education, Culture, Sports, Science and Technology of Japan

[1]To whom correspondence should be addressed: Dept. of Biochemistry, Asahikawa Medical College, Midorigaoka-higashi, Asahikawa, 078-8510, Japan. Tel.: 81-166-68-2353; Fax: 81-166-68-2359; E-mail: daiho@asahikawa-med.ac.jp.

[2]The abbreviations used are: SERCA1a, adult fast-twitch skeletal muscle sarcoplasmic reticulum Ca^{2+}-ATPase; SR, sarcoplasmic reticulum; *E*P, phosphoenzyme; *E*1PCa_2, ADP-sensitive phosphoenzyme with occluded Ca^{2+}; *E*2PCa_2, ADP-insensitive phosphoenzyme with occluded Ca^{2+}; *E*2P, ADP-insensitive phosphoenzyme; TG, thapsigargin; MOPS, 3-(*N*-morpholino)propanesulfonic acid; prtK, proteinase K.

FIGURE LEGENDS

FIGURE 1. **Ca^{2+}-transport cycle of SERCA.**

FIGURE 2. **Crystal structures of SERCA1a.** The coordinates for structures *E*1Ca_2·AlF_4^-·ADP (the analog of the transition state of phosphorylation, *left*) and *E*2·BeF_3^- (the analog of the *E*2P ground state, *right*) were obtained from Protein Data Bank (PDB accession code 1T5T (17) and 2ZBE (21), respectively). *a*, the cytoplasmic domains N (nucleotide binding), P (phosphorylation), A (actuator), 10 transmembrane helices (M1-M10), phosphorylation site Asp^{351}, and $TGES^{184}$ on the A domain are indicated. Cleavage sites by trypsin (*T1* (Arg^{505}) and *T2* (Arg^{198} on the *Val*^{200} *loop* ($DPR^{198}AV^{200}NQD$)) and by proteinase K (prtK) (Leu^{119} on the top part of M2 and Thr^{242} on the A/M3-linker) are shown. *Arrows* indicate approximate motions of the A and P domains, M2, and M1' from *E*1Ca_2·AlF_4^-·ADP to *E*2·BeF_3^-. Note the large rotation of the A domain and the inclination of the P and A domains and M2. In the *E*2P state, the A and P domains interact at three regions; at the $T^{181}GES$ loop with the residues around Asp^{351}, at the Val^{200} loop (Asp^{196}-Asp^{203}) with polar residues of the P domain, and at Leu^{119}/Tyr^{122} on the top part of M2 with the A, P, and N domains. In *E*2·BeF_3^-(TG) (2ZBF (21), supplemental Fig. S5), Leu^{119}/Tyr^{122} produce the Tyr^{122}-hydrophobic cluster with five other hydrophobic residues, Ile^{179}/Leu^{180}/Ile^{232} of the A domain and Val^{705}/Val^{726} of the P domain. In *E*2·BeF_3^- without TG, the cluster structure is rather loose (as the side chains of Leu^{119}/Tyr^{122} are pointing away from the hydrophobic cluster), but Leu^{119}/Tyr^{122} produce a more extended interaction network involving Thr^{430} of the N domain and the hydrophobic cluster (see more details in supplemental Fig. S5). *b*, the catalytic site is enlarged and the residues involved in the Mg^{2+} (site I) are depicted. The Val^{679}-Lys^{686} region of the P domain is not depicted for simplicity (because it is positioned over the region of interest).

FIGURE 3. **Inhibition of *E*P formation from ATP by metal fluoride.** *A* and *C*, microsomes expressing the wild type or mutant 4Gi-46/47 (0.35 mg/ml) were treated at 25 °C for 30 min with metal fluoride in the presence of 0.01 mM Ca^{2+} (0.01 mM $CaCl_2$ without EGTA) in 3 mM KF plus 50 μM $BeSO_4$ or $AlCl_3$, 0.1 M KCl, and 50 mM MOPS/Tris (pH 7) with (*black bar*) or without (*white bar*) 15 mM $MgCl_2$. Subsequently, the samples were diluted 10-fold and phosphorylated at 0 °C for 15 s with 10 μM [γ-^{32}P]ATP in 1 μM A23187, 0.1 mM Ca^{2+} (0.5 mM $CaCl_2$ with 0.4 mM EGTA), 7 mM $MgCl_2$, 0.1 M KCl, and 50 mM MOPS/Tris (pH 7), and the amount of *E*P formed was determined. The amount of *E*P formed with the wild type in the control sample, *i.e.* incubated without the fluoride compounds and Mg^{2+}, (4.7 nmol/mg of the expressed SERCA1a) was normalized to 100%. The amount of *E*P formed with the mutant 4Gi-46/47 in the control sample was almost the same as that of wild type. *B* and *D*, microsomes were treated with metal fluoride in the absence of Ca^{2+} (1 mM EGTA without added $CaCl_2$) and in the presence of the indicated concentration of $MgCl_2$. Subsequently, the samples were diluted 2.5-fold with a solution containing 1 μM A23187, 0.1 M KCl,

50 mM MOPS/Tris (pH 7), and EGTA (to give 1 mM, *white bar*) or $CaCl_2$ (to give 10 mM Ca^{2+}, *black bar*), and incubated at 25 °C for 1 h. The samples were then further diluted 10-fold and phosphorylated with 10 μM [γ-^{32}P]ATP and 0.1 mM Ca^{2+} as in *A* and *C*, and the amount of *E*P formed was determined.

FIGURE 4. **Be^{2+} dependence of the rate of *E*P inhibition by BeF_x in 0.01 mM Ca^{2+}.** *A*, microsomes expressing the wild type or mutant 4Gi-46/47 were incubated for various periods in 0.01 mM Ca^{2+} and 1 mM KF with various concentrations of $BeSO_4$, otherwise as in Fig. 3*A* and *C* for BeF_x-treatment. The samples were then diluted 10-fold and phosphorylated with 10 μM [γ-^{32}P]ATP and the amount of *E*P formed was determined, as in Fig. 3*A* and *C*. *Solid lines* show the least squares fit to a single exponential. In *B*, the rate constants obtained in *A* were plotted versus the concentration of Be^{2+} added. The linear fit to the data gave a slope of 0.123 $min^{-1}\mu M^{-1}$.

FIGURE 5. **Mg^{2+} dependence of the rate of *E*P inhibition by BeF_x in 0.01 mM Ca^{2+}.** *A*, microsomes expressing the mutant 4Gi-46/47 were incubated for various periods in 0.01 mM Ca^{2+}, 1 mM KF, 10 μM $BeSO_4$, and various concentrations of $MgCl_2$, otherwise as in Fig. 3*A* and *C* for BeF_x-treatment. The samples were then diluted 10-fold and phosphorylated with 10 μM [γ-^{32}P]ATP and the amount of *E*P formed was determined, as in Fig. 3*A* and *C*. *Solid lines* show the least squares fit to a single exponential. In *B*, the rate constants obtained in *A* were plotted versus the concentration of Mg^{2+} added. $K_{0.5}$ for the Mg^{2+} activation and Hill coefficient obtained by fitting to the Hill equation (*solid line*) were 4.9 mM and 2.3, respectively.

FIGURE 6. ***E*P inhibition by Mn^{2+} and BeF_x in 0.01 mM Ca^{2+} without Mg^{2+}.** Microsomes expressing the wild type or mutant 4Gi-46/47 were treated with 1 mM F^- plus 50 μM Be^{2+} or Al^{3+} in 0.01 mM Ca^{2+} and in the absence (*white bar*) or presence (*black bar*) of 2 mM $MnCl_2$ (in place of $MgCl_2$), otherwise as in Fig. 3*A* and *C*. The samples were then diluted 10-fold and phosphorylated with 10 μM [γ-^{32}P]ATP and the amount of *E*P formed was determined, as in Fig. 3*A* and *C*.

FIGURE 7. ***E*P inhibition by 10 mM Ca^{2+} and BeF_x without Mg^{2+} and Mn^{2+}.** Microsomes expressing the wild type or mutant 4Gi-46/47 were treated with 1 mM F^- plus 50 μM Be^{2+} or Al^{3+} in 0.01 or 10 mM $CaCl_2$ without Mg^{2+} and Mn^{2+}, otherwise as in Fig. 3*A* and *C*. The samples were then diluted 10-fold and phosphorylated with 10 μM [γ-^{32}P]ATP and the amount of *E*P was determined, as in Fig. 3*A* and *C*.

FIGURE 8. **Ca^{2+} occlusion in $E2Ca_2{\cdot}BeF_3^-$ of the mutant 4Gi-46/47 formed from $E1Ca_2$ (*A*) and from $E2{\cdot}BeF_3^-$ (*B*).** *A*, microsomes (0.2 mg/ml) expressing the mutant 4Gi-46/47 were incubated for various periods at 25 °C in 10 μl of a mixture containing 0.01 mM $^{45}CaCl_2$, 1 mM KF, 1 μM $BeSO_4$, 15 mM $MgCl_2$, 0.1 M KCl, 50 mM MOPS/Tris (pH 7). The mixture was then diluted 200-fold at 0 °C with a "washing solution" containing 2 mM EGTA, 5 μM A23187, 0.1 M KCl, 7 mM $MgCl_2$, and 50 mM MOPS/Tris (pH 7.0), subjected to membrane filtration, and washed rapidly with 6 ml of the "washing solution" for 4 s at 0 °C. For determination of *E*P, the above BeF_x-incubation was made with $^{40}Ca^{2+}$ instead of $^{45}Ca^{2+}$ otherwise as above, and the sample was diluted 10-fold and phosphorylated with 10 μM [γ-^{32}P]ATP at 0 °C for 15 s as in Fig. 3*C*. The sample was then further diluted 20-fold at 0 °C with the "washing solution", immediately filtered as above, and washed rapidly with ice-cold trichloroacetic acid containing P_i. The *E*P level was not changed during the above sample handling because the decay of *E*P ($E2PCa_2$) is almost completely blocked in the mutant (14). The amount of $^{45}Ca^{2+}$ specifically bound and occluded (■) and that of $E^{32}P$ formed (○) in the expressed SERCA1a mutant were obtained by subtracting the background levels determined by including 1 μM TG in the BeF_x incubation mixture. The values presented are the mean ± S.D. (n = 5). *Inset*, the amount of *E*P formed was replotted versus that of occluded Ca^{2+} with the BeF_x-treatment. The *solid line* represents the linear least squares fit. The y and x intercepts gave 4.3 and 8.4 nmol/mg of the expressed SERCA1a for the amounts of *E*P and of Ca^{2+} occluded, respectively. *B*, for formation of $E2{\cdot}BeF_3^-$, microsomes (1 mg/ml) expressing the mutant 4Gi-46/47 were incubated at 25 °C for 30 min with 1 mM KF and 20 μM $BeSO_4$ in 1 mM EGTA, 7 mM $MgCl_2$, 50 mM LiCl, and 50 mM MOPS/Tris (pH 7). Then, the mixture was diluted 2.5-fold with a solution containing 7 mM $MgCl_2$, 50 mM LiCl, 50 mM MOPS/Tris (pH 7), 5 μM Ca^{2+} ionophore A23187, and various concentration of $^{45}CaCl_2$ to give the indicated final $^{45}Ca^{2+}$ concentrations. After incubating at 25 °C for 1 min, the mixture was further diluted with 400-fold of the "washing solution" containing the excess EGTA, filtered, and washed

with the "washing solution" as above. The amount of $^{45}Ca^{2+}$ specifically bound and occluded in the SERCA1a was obtained by subtracting the nonspecific Ca^{2+}-binding, which was determined without KF in the BeF_x-treatment mixture. In the fitting to the Hill equation (*solid line*), the maximum amount of occluded Ca^{2+}, $K_{0.5}$ for the Ca^{2+} activation, and Hill coefficient were obtained as 7.7 nmol/mg of the expressed SERCA1a, 0.1 mM, and 1.6, respectively. The values presented are the mean ± S.D. (n = 7).

FIGURE 9. **Stability of *E*2Ca_2·BeF_3^- of the mutant 4Gi-46/47.** *A*, the complex *E*2Ca_2·BeF_3^- was produced with the mutant 4Gi-46/47 for 30 min at 25 °C in 0.05 mM $^{45}CaCl_2$, 1 mM KF, 50 μM $BeSO_4$, and 15 mM $MgCl_2$, otherwise as in Fig. 8*A*. Then a small volume of A23187 was added to give 1 μM, and the incubation was further continued at 25 °C. At various times, the amount of $^{45}Ca^{2+}$ specifically bound and occluded in the mutant was measured following an EGTA wash, and by subtracting the background levels determined in the absence of F^- in the incubation mixture, otherwise as in Fig. 8*A*. *Inset*, after the formation of *E*2Ca_2·BeF_3^- as above, the sample was diluted 100-fold at 25 °C with a solution containing 1 μM A23187, 0.1 M KCl, 7 mM $MgCl_2$, 2 mM EGTA, and 50 mM MOPS/Tris (pH 7.0) (without BeF_x) in the absence (○) or presence (●) of 1 μM TG, and incubated for various periods and the amount of $^{45}Ca^{2+}$ specifically bound and occluded in the mutant obtained as above. The values presented are the mean ± S.D. (n = 7). *Solid lines* in *inset* show the least squares fit to a single exponential, and the decay rate constants thus obtained are 7.0 (○) and 14.0 (●) h^{-1} without and with TG, respectively. In the *main panel* and *inset*, the amount of Ca^{2+} occluded in the complex *E*2Ca_2·BeF_3^- at time zero (immediately before starting the long incubation or the dilution) was normalized to 100%.

Figure 1

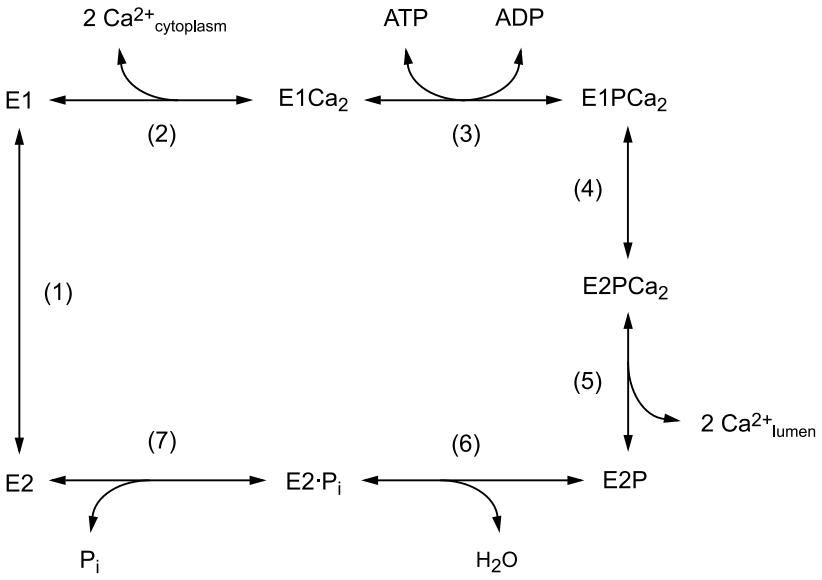
2 Ca2+cytoplasm
ATP
ADP
E1
E1Ca2
E1PCa2
(2)
(3)
(4)
(1)
E2PCa2
(5)
2 Ca2+lumen
(7)
(6)
E2
E2·Pi
E2P
Pi
H2O

Figure 2

a

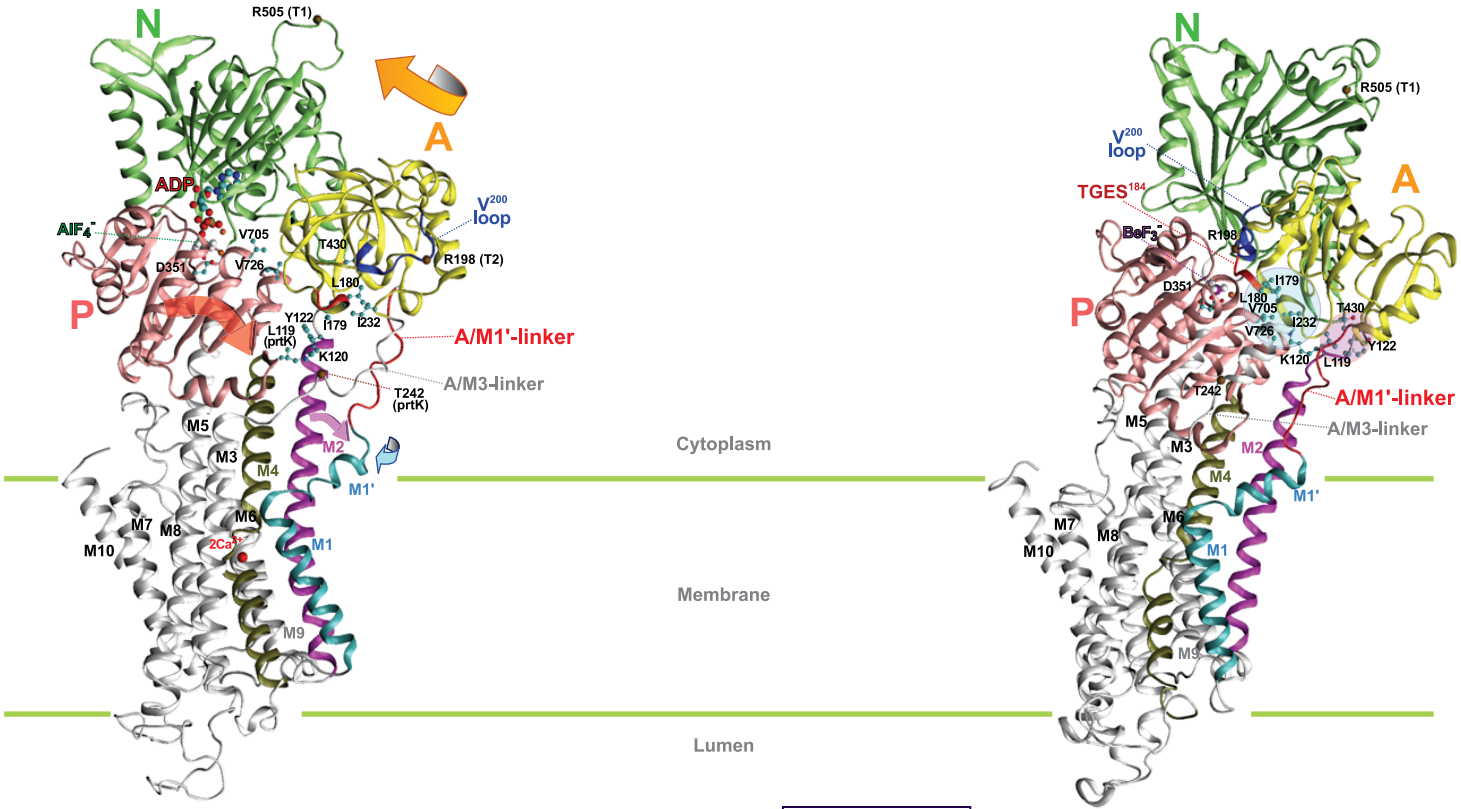

E1PCa$_2$·ADP·Mg‡ (E1Ca$_2$·AlF$_4^-$·ADP) ⇨ E1PCa$_2$·Mg (E1Ca$_2$·BeF$_3^-$) ⇨ **E2PCa$_2$·Mg** ⇨ E2P·Mg (E2·BeF$_3^-$)

b

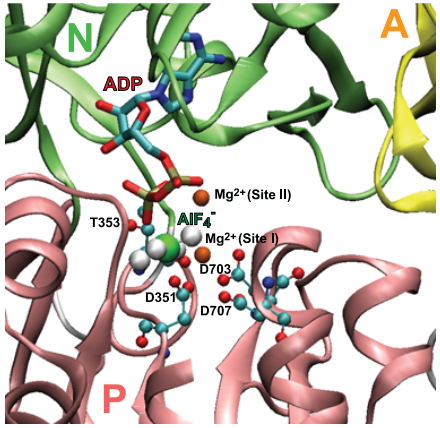

E1PCa$_2$·ADP·Mg‡ (E1Ca$_2$·AlF$_4^-$·ADP)

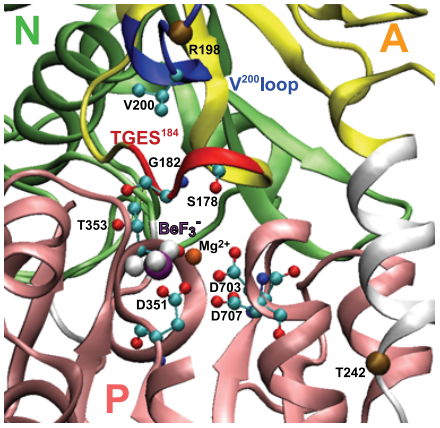

E2P·Mg (E2·BeF$_3^-$)

Figure 3

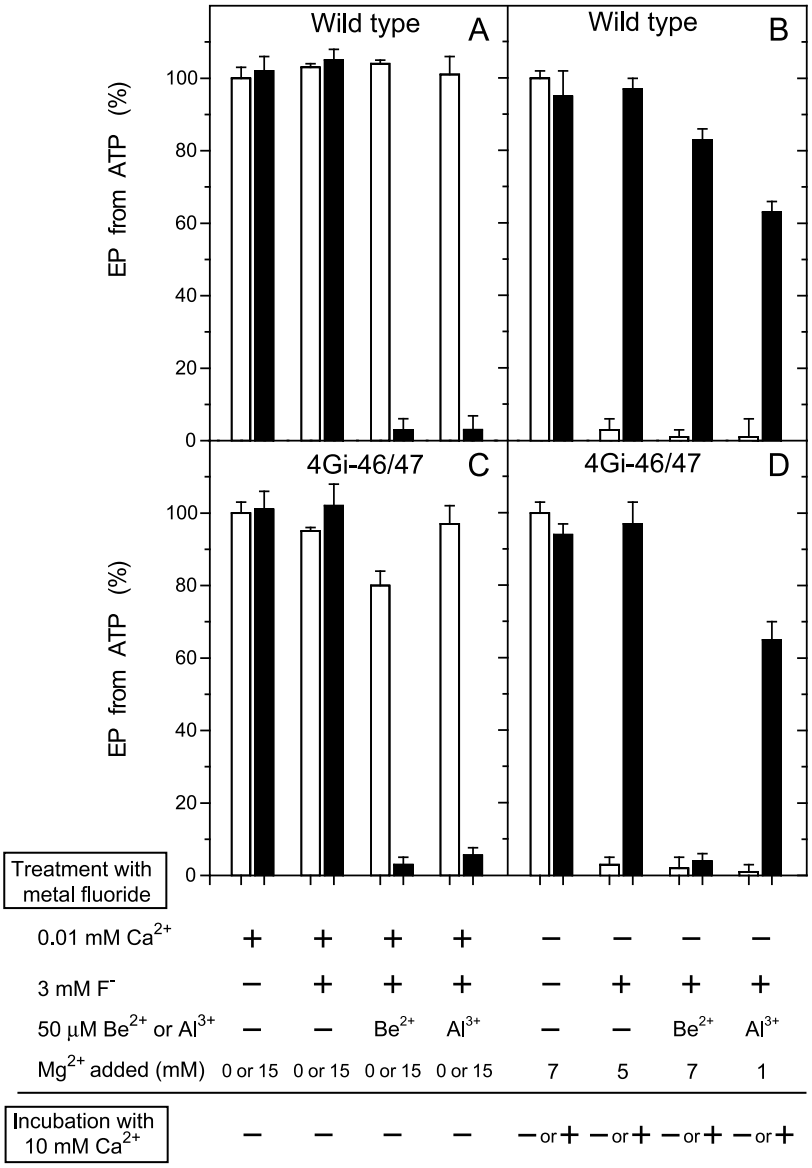
Wild type
A
Wild type
B
4Gi-46/47
C
4Gi-46/47
D
EP from ATP (%)
EP from ATP (%)
0
20
40
60
80
100
Treatment with metal fluoride
0.01 mM Ca2+
3 mM F-
50 μM Be2+ or Al3+
Mg2+ added (mM)
0 or 15
0 or 15
0 or 15
0 or 15
7
5
7
1
Incubation with 10 mM Ca2+
− or +

Figure 4

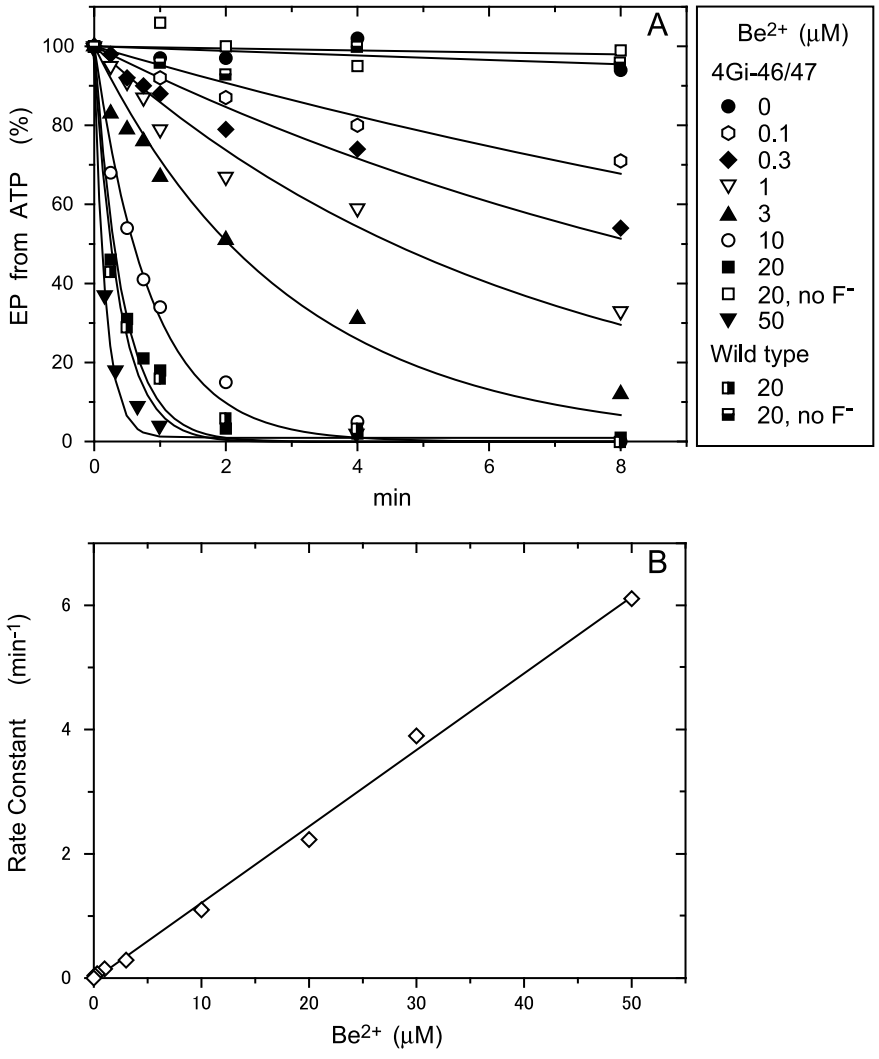
A
EP from ATP (%)
min
Be2+ (μM)
4Gi-46/47
0
0.1
0.3
1
3
10
20
20, no F-
50
Wild type
20
20, no F-
B
Rate Constant (min-1)
Be2+ (μM)

Figure 5

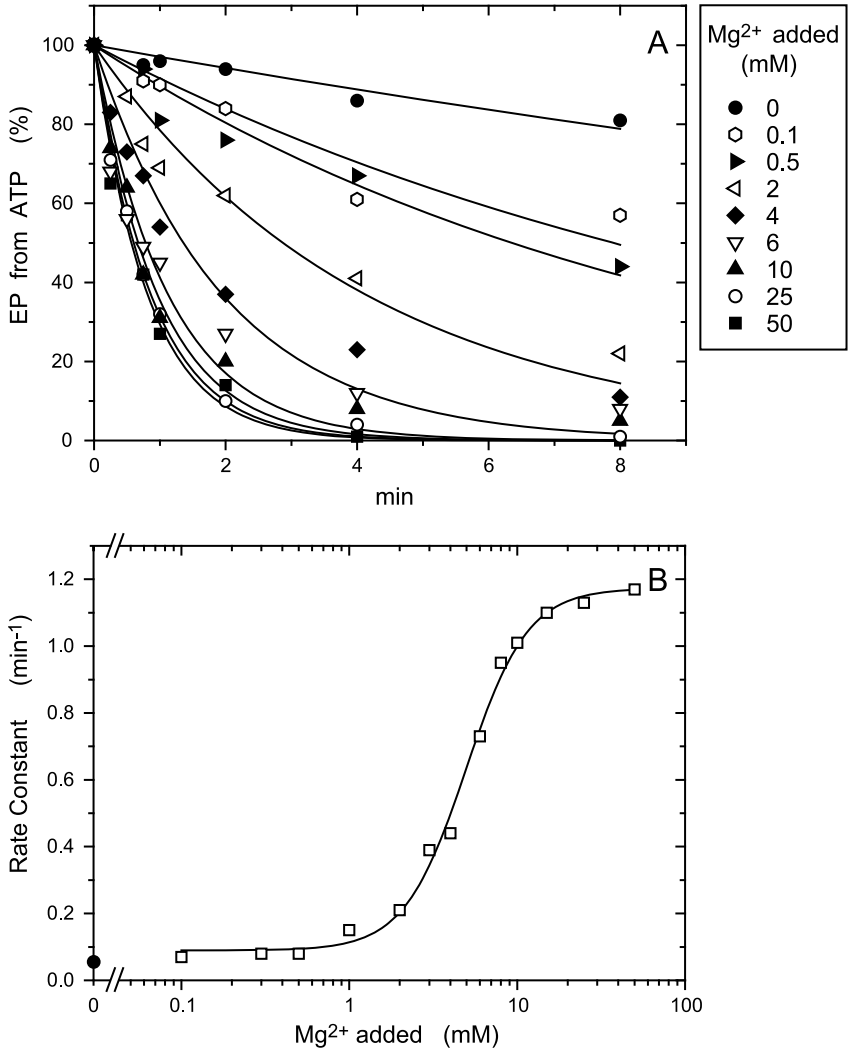
A
EP from ATP (%)
min
Mg2+ added (mM)
0
0.1
0.5
2
4
6
10
25
50
B
Rate Constant (min-1)
Mg2+ added (mM)

Figure 6

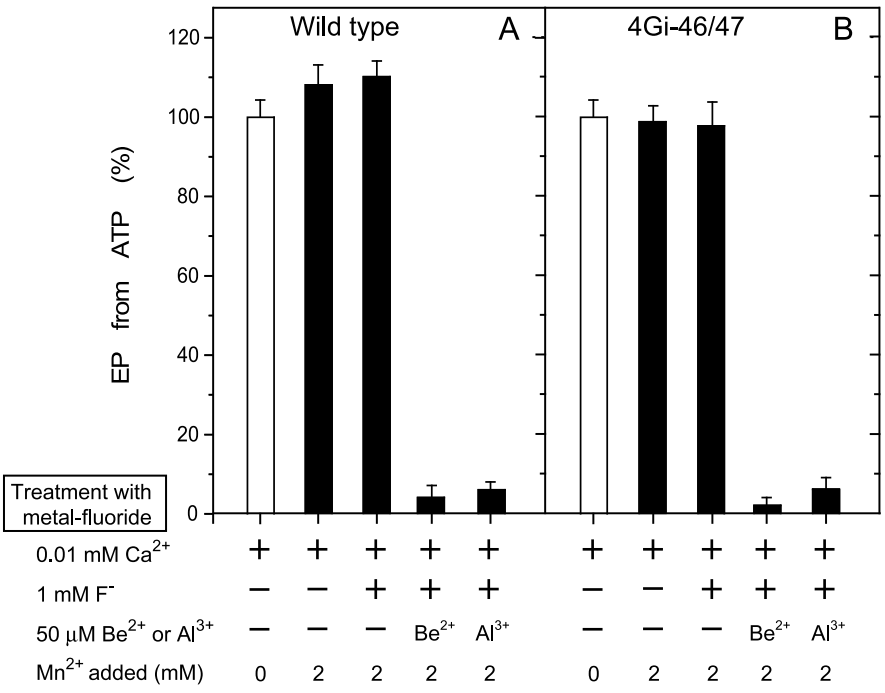
Wild type
A
4Gi-46/47
B
EP from ATP (%)
120
100
80
60
40
20
0
Treatment with metal-fluoride
0.01 mM Ca2+
1 mM F-
50 µM Be2+ or Al3+
Mn2+ added (mM)
Be2+
Al3+
0
2

Figure 7

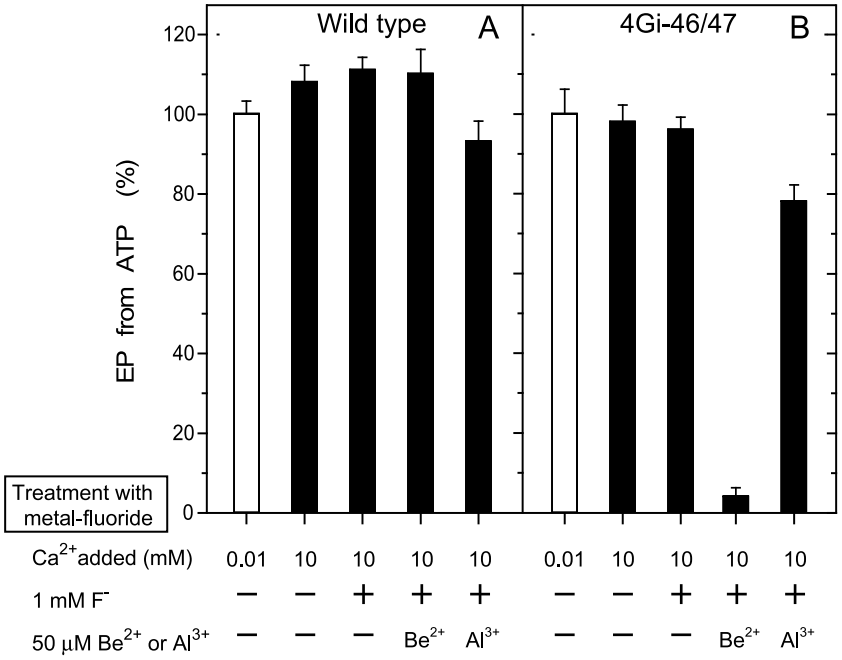
Wild type
A
4Gi-46/47
B
EP from ATP (%)
120
100
80
60
40
20
0
Treatment with metal-fluoride
Ca2+added (mM)
0.01 10 10 10 10 0.01 10 10 10 10
1 mM F-
− − + + + − − + + +
50 μM Be2+ or Al3+
− − − Be2+ Al3+ − − − Be2+ Al3+

Figure 8

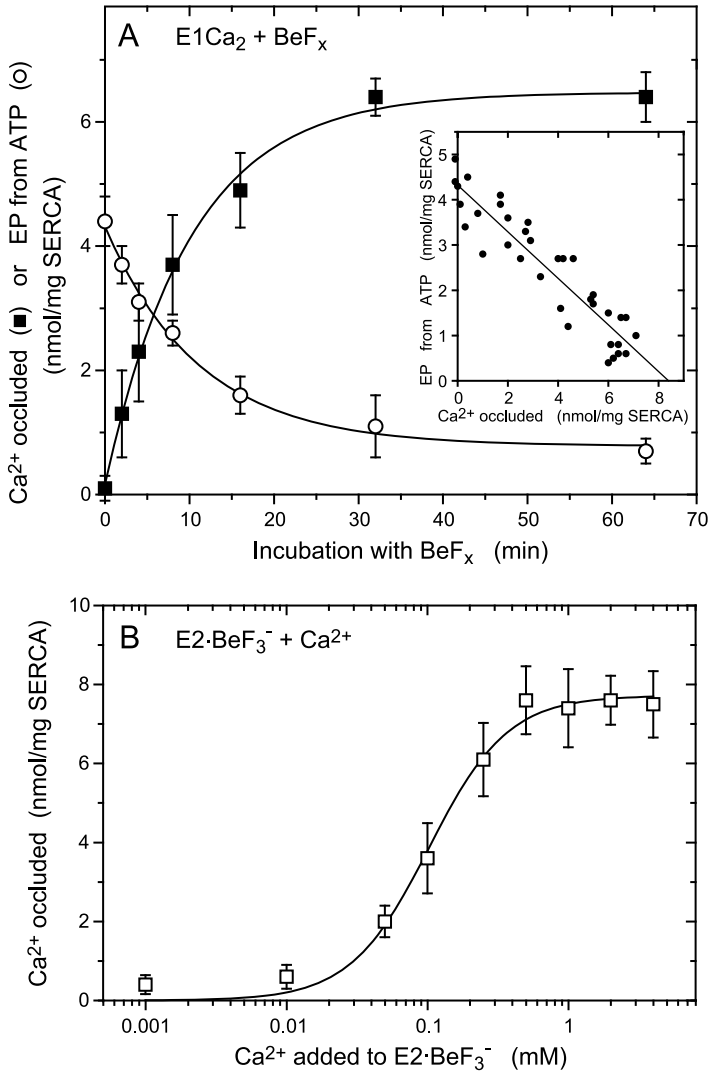
A
E1Ca2 + BeFx
Ca2+ occluded (■) or EP from ATP (○)
(nmol/mg SERCA)
Incubation with BeFx (min)
EP from ATP (nmol/mg SERCA)
Ca2+ occluded (nmol/mg SERCA)
B
E2·BeF3- + Ca2+
Ca2+ occluded (nmol/mg SERCA)
Ca2+ added to E2·BeF3- (mM)

Figure 9

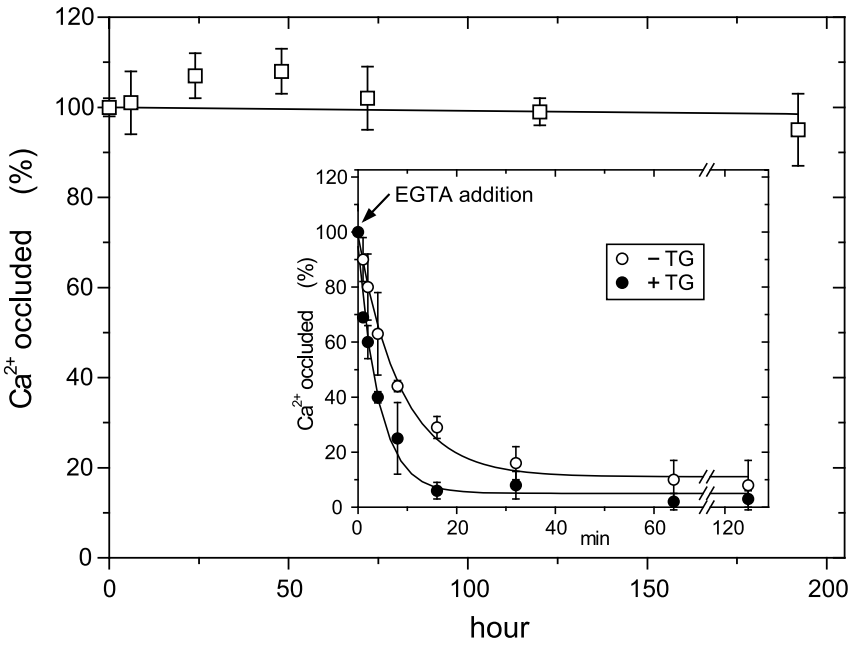
120
100
80
60
40
20
0
Ca2+ occluded (%)
0
50
100
150
200
hour
EGTA addition
− TG
+ TG
Ca2+ occluded (%)
min
0
20
40
60
120